

# Optimization of Amplitude-Modulated Pulses for Bloch-Siebert Based $B_1$ Mapping

Qi Duan<sup>1</sup>, Peter van Gelderen<sup>1</sup>, Souheil J. Inati<sup>2</sup>, and Jeff H. Duyn<sup>1</sup>

<sup>1</sup>AMRI, LFMI, National Institute of Neurological Disorders and Stroke, National Institutes of Health, Bethesda, Maryland, United States, <sup>2</sup>FMRIF, National Institute of Mental Health, National Institutes of Health, Bethesda, Maryland, United States

**Target Audience** MR physicists, engineers.

## Purpose

Reducing RF power deposition with Bloch-Siebert (BS)-based  $B_1$  mapping<sup>1</sup> is an active area of research<sup>2-6</sup>. The recent realization that both the sensitivity and the SNR of BS methods are proportional  $\gamma^2 \text{SAR}/\omega_{RF}$  has suggested that BS pulse optimization should be done under a constant energy assumption rather than a fixed amplitude assumption. Here, we followed this approach, while simultaneously considering the effectiveness of gradient crushers in minimizing signal excitation and saturation effects associated with the BS pulse.

## Methods

**Pulse Optimization:** We focused on an amplitude-modulated BS pulse and gradient-echo (GRE) readout<sup>3</sup> (Fig.1), and considered the effect that increased BS pulse and crusher duration minimize signal excitation, while increasing signal loss due to  $T_2^*$  decay. This optimization depends on the scanner gradient specs, as well as on background field gradients. The following three-step optimization is proposed: 1) design of BS pulse shape under constant-energy assumption for varying pulse duration (simulation); 2) crusher optimization for each of the optimal pulses at each pulse duration (using *in vivo* MRI for realistic background fields); 3) angle-to-noise ratio (ANR) measurement of each optimal pulse-crusher combination (*in vivo* for realistic background fields, and because of effects such as drift and motion). Below, we demonstrate this optimization for  $\Delta f_{RF}=500\text{Hz}$ .

Pulse optimization under constant energy assumption is mathematically equivalent to a spectrum concentration problem, whose solutions are prolate spheroidal sequences<sup>7</sup> (only 0<sup>th</sup> order, DPSS, demonstrated here). A fixed number (1000) of pulse support points was used, while the time-half-bandwidth product ( $thbw$ ) was varied from 0.1 to 10. For each pulse duration (2ms to 9ms with 1ms step), the pulse shape generating the least amount of direct excitation in the 200-800Hz band (based on estimated  $B_0$  variations in the head at 7T<sup>3</sup>) via Bloch-simulation. For each optimal pulse at a particular duration, the minimal crusher duration was found *in vivo* by setting the RF excitation pulse to zero and incrementally reducing crusher moment until signal became visible above background noise. Finally, ANR was measured for each pulse-crusher combination by calculating the ratio of mean and standard deviation of 10 repeat measurements.

**MRI experiments:** IRB-approved MRI experiments were performed on a Siemens Magnetom 7T using FOV 256mm, imaging matrix 64x64, slice thickness=5mm. The reference  $B_1$  map was acquired with a 8ms 8kHz Fermi pulse (nominal  $\phi_{BS}=60^\circ$ , TR = 615ms, 10 averages, maximum SAR). For demonstration purpose, both DPSS pulses and a previously optimized pulse under constant amplitude assumption (QDAPX)<sup>3</sup> went through crusher optimization and ANR measurement, with  $\Delta f_{RF}=500\text{Hz}$ , 2-9ms, 64% of maximal SAR, nominal  $\phi_{BS}=60^\circ$ , minimum TE, TR=60ms. The ANR of an 8ms 8kHz Fermi pulse under the same conditions was used as reference. The nominal flip angle was set to the Ernst angle. Data were collected from five healthy volunteers.

## Results and Discussion

DPSS pulses generally required smaller crushers than the QDAPX pulse for all pulse durations. ANRs of DPSS pulse and QDAPX pulse from one subject, relative to the Fermi pulse, are shown in Fig.2b. For both DPSS and QDAPX pulse, RMS ANR ratios were maximized with 8ms pulse duration (7.8 and 4.5 respectively), with corresponding relative errors in  $B_1$  as 1.0%, 1.1%, and 1.5% respectively. This suggests that the 8ms DPSS pulse is optimal terms of ANR. This is confirmed by relative  $B_1$  maps, relative  $B_1$  errors, and ANR maps (Fig.3). Results from other subjects are very similar.

We find that shorter TE does not necessarily translate into a higher SNR in the  $B_1$  map, because of competition between  $T_2^*$  decay and the saturation effect from the BS pulses. This suggests that in the BS pulse design, the effect of different pulse duration cannot be simply considered as a  $T_2^*$  penalty on imaging SNR. Such disassociation between TE and SNR in the  $B_1$  map suggests that proper evaluation of the SNR performance for different BS pulses has to be done *in vivo* after proper crusher optimization. BS pulse optimization under a constant energy assumption decouples the direct excitation minimization from the optimization of BS shift. It also removes the need to predefine an arbitrary threshold for the stop-band response. In fact, the optimal 8ms DPSS pulse found by the experiments has higher stop-band response than the Fermi and the QDAPX pulse for most of the high frequency spectrum. This is not only suggesting that tailoring the boundary of the stop-band in optimization could further improve the pulse, but also shows the difficulty in properly defining a threshold that is sufficient for applications. This further stresses the point that BS pulse optimization, and choice of frequency offset, require careful consideration of the actual  $B_0$  variations in the object under study. Although an *in vivo* calibration of crushers is necessary in this proposed method, we found the optimal solution was quite consistent across a group of five subjects for a particular choice of  $B_1$  SNR and measurement time. In the current optimization, the range of TE was not limited. It is also possible to reformulate the optimization problem under a constant TE assumption. This, however, generally requires the pulses operate at different energy level, which is out of the scope of this study.

## Conclusion

A new BS pulse optimization framework under constant energy assumption with consideration of crushers is proposed and a resulting sensitivity improvement is demonstrated *in vivo*.

## Reference

1. Sacolick LI, Wiesinger F, Hancu I, Vogel MW.  $B_1$  mapping by Bloch-Siebert shift. *Magn Reson Med*. May 2010;63(5):1315-1322.
2. Basse-Lusebrink TC, Kampf T, Fischer A, et al. SAR-reduced spin-echo-based Bloch-Siebert  $B_1$  (+) mapping: BS-SE-BURST. *Magn Reson Med*. Nov 30 2012;68(2):529-536.
3. Duan Q, van Gelderen P, Duyn J. Improved Bloch-Siebert based  $B_1$  mapping by reducing off-resonance shift. *NMR Biomed*. Jan 28 2013;26(9):1070-1078.
4. Jankiewicz M, Gore JC, Grissom WA. Improved encoding pulses for Bloch-Siebert  $B_1$ (+)-mapping. *J Magn Reson*. Jan 2013;226:79-87.
5. Khalighi MM, Rutt BK, Kerr AB. Adiabatic RF pulse design for Bloch-Siebert  $B_1$  + mapping. *Magn Reson Med*. Oct 5 2012;DOI: 10.1002/mrm.24507.
6. Nehrke K, Bornert P. Fast  $B_1$  Mapping using a STEAM-based Bloch-Siebert Preparation Pulse. *19th Annual Meeting & Exhibition of ISMRM*. Vol Montreal, CA2011:4411.
7. Slepian D, Pollak H. Prolate-spheroidal wave functions, Fourier analysis and uncertainty - I. *Bell System Technical Journal*. 1961;40:43-64.

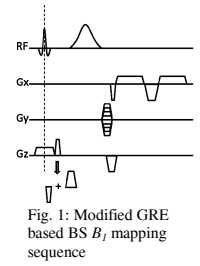


Fig. 1: Modified GRE based BS  $B_1$  mapping sequence

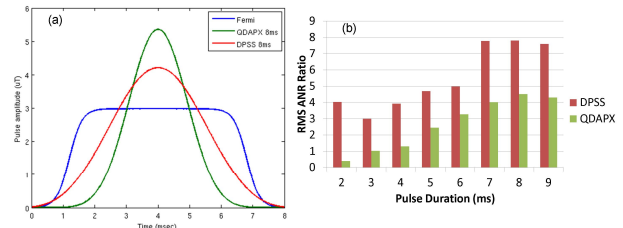


Fig. 2: (a) pulse shapes; (b) RMS ANR ratio

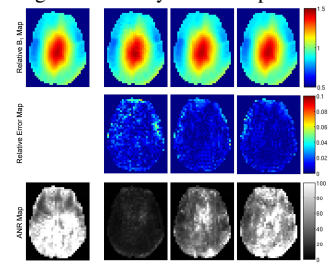


Fig. 3: *In vivo*  $B_1$  mapping, errors, and ANR